Predictive Direct Control of SPMS Generators Applied to the Machine Side Converter of an OWC Power Plant

Mohammad Ebrahim Zarei; Dionisio Ramirez; Carlos Veganzones; Jaime Rodriguez

To cite this version:

M. E. Zarei, D. Ramirez, C. Veganzones and J. Rodriguez, "Predictive Direct Control of SPMS Generators Applied to the Machine Side Converter of an OWC Power Plant," in *IEEE Transactions on Power Electronics*, vol. 35, no. 7, pp. 6719-6731, July 2020, doi: 10.1109/TPEL.2019.2956738.

Published Version.

Published 2020 July 01

Archivo Digital UPM houses in digital format the academic and scientific documentation (theses, pfc, articles, etc.) generated at the institution and makes it accessible through the Internet, within the framework of the Budapest Open Access Initiative and the Berlin Declaration, of which the Universidad Politécnica de Madrid is a signatory.

El A**rchivo Digital UPM** alberga en formato digital la documentación académica y científica (tesis, pfc, artículos, etc..) generada en la institución y la hace accesible a través de Internet, en el marco de la Iniciativa por el Accesso Abierto de Budapest y la Declaración de Berlín, de la que es signataria la Universidad Politécnica de Madrid.

Predictive Direct Control of SPMS Generators applied to the Machine Side Converter of an OWC power plant

Mohammad Ebrahim Zarei, Dionisio Ramirez, Carlos Veganzones and Jaime Rodriguez

Abstract- **A new strategy framed in the field of model predictive direct current control (MPDCC) applied to surface permanent magnet synchronous generator (SPMSG) is presented. Compared to conventional space vector control systems, the proposed predictive strategy reduces the number of PI regulators and maintains the advantages of a fixed switching frequency. It also performs a faster response providing a smooth electromagnetic torque and smooth active and reactive power control. The dynamic performance of the proposed control is firstly analyzed by means of simulations in MATLAB Simulink environment and then compared with two other model predictive controls (MPC). Also, the performance of the control is analyzed in simulation using a simple model of an oscillating water column (OWC) power plant. This application was chosen because it is a difficult case study that demands a fast torque control to handle the power take-off (PTO) system. Later, the proposed method is tested in a customized SPMSG based laboratory setup.**
This paper is accompanied by a video.[1]

I. Introduction

Predictive control systems were started to develop in the late 1980's to deal with the limitations of the traditional control systems such as field-oriented control (FOC) and direct torque control (DTC) methods. The performance of the conventional DTC, based on a switching table, is related to the sample time of the microcontroller [1]. As a result, the ripple of the torque and other variables is high if a high sampling time is not applied, in spite of the fact that DTC method is fast and has a robust structure compared to the FOC control [2]. The FOC method, often present in the machine side converter (MSC) and the grid side converter (GSC) of wind turbines, etc., features fixed switching frequency and low power ripple. However, the control provides a slow response and any perturbation in the system or in the grid could deteriorate the performance of the controller [3], [4].

In recent years, different model based predictive controls (MPCs) for voltage source converters have been introduced and applied to renewable energy sources and electrical drives. In this control, the model of the system is considered, and according to a cost function and the control objectives, an optimal voltage vector is chosen [5]. With this technique, the phase locked loop (PLL) and the space vector modulation code are unnecessary. In classical MPC, only one voltage vector is applied in every switching interval [6]; as a result, a high ripple appears in the control variables. The switching frequency of this method, similarly to DTC, is variable. Additionally, the results look alike to those obtained with the DTC method [7].

Many alternative strategies have been introduced to overcome these disadvantages such as the duty cycle optimization based on two vector MPC (TWMPC) [8]-[9] where a nonzero, and a zero vector are applied in each interval. Also, a reduced ripple based on TWMPC [10]-[11], a multi-vector predictive control [12]-[13] and predictive power control based on four vectors [14] were also presented and comprise the short horizon MPC. A long horizon direct torque MPC was suggested in [15]-[16] where an intelligent calculation method is needed. Although this method features promising performances, the implementation in a real system is difficult nowadays.

As aforementioned, an effective and easy implementation of MPC featuring fixed switching frequency and low variable ripple is highly demanded by the industry, especially in electrical generation.

The case study chosen to check the performance of the proposed MPDCC is the machine side converter of an OWC-based power plant. The reason is that it presents very demanding control requirements that combine electrical aspects and fast-dynamic response to cope with fast and large variations of torque generated by the waves in the SPMSG shaft of the power take-off (PTO).

This paper presents several tests carried out using an oscillating water column (OWC) based power plant emulator [17]-[18]. OWC based power plants comprise an air chamber, a wells turbine and a rotary electric generator [19]-[21] (Fig. 1).

The pressure exerted by the wave on the air inside a chamber generates an air flow that drives an air turbine. As the water level inside the chamber increases or decreases, it pushes the air in and out of the chamber through a turbine driving an electric generator. Despite the alternating air flow, most of the PTO systems used with OWC devices maintain a continuous direction of rotation, for instance, using a Wells turbine.

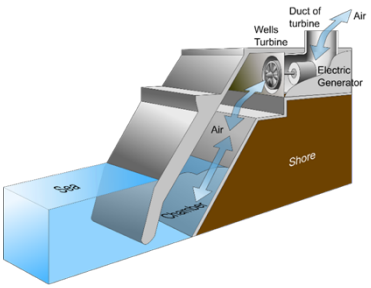

Fig. 1 Schematic representation of an OWC power plant.

This paper presents a model predictive direct current control (MPDCC) based on four voltage vectors for SPMS Generators. The proposed strategy features fixed switching frequency, fast dynamic response and low ripple in the control variables, what make it very suitable to make OWC power plants using SMPMG track the maximum efficiency point in every situation. The paper is organized as follows. In Section II, the proposed MPDCC for the SPMSG is presented, and the selection of voltage vector sequences and the calculation of the optimal duration time of vectors are explained. After that, the OWC based power plant emulator model is described in section III. Then, the proposed predictive current control is evaluated using Matlab Simulink, and the simulation results are shown in Section IV. Section V shows the experimental test carried out in the laboratory using an OWC-based power plant emulator, and the effectiveness of the proposed method is checked during a four minutes long test. At the end of the paper, Section VI presents the conclusions.

II. Model Predictive Direct Current control for the SPMSG

The model predictive direct current control for the SPMSG is presented in this section which uses four voltage vectors in every switching interval. First, the current slopes, the vector sequences and the duration times are described. Then, the sector identification algorithm, which selects the best vector sequence, is represented.

A. Current slopes and vector sequences

The SPMSG dynamic equations in rotor rotating reference frame, d-q frame, can be presented as [22]

$$u_{sd} = R_s i_{sd} + \frac{d}{dt}\lambda_{sd} - \omega_m \lambda_{sq} \quad (1)$$

$$u_{sq} = R_s i_{sq} + \frac{d}{dt}\lambda_{sq} + \omega_r \lambda_{sd} \quad (2)$$

where $u_s, i_s, \lambda_s, \omega_r$ and R_s are stator voltage vector, stator current vector, stator flux, electrical rotor speed and stator resistance, respectively. The stator flux of SPMSG in the d-q frame is

$$\lambda_{sd} = L_s i_{sd} + \lambda_f \quad (3)$$

$$\lambda_{sq} = L_s i_{sq} \quad (4)$$

where λ_f and L_s represent permanent magnet flux and stator inductance, respectively. The torque equation can be expressed as

$$T_e = \frac{3}{2} p\left(\lambda_{sd} i_{sq} - \lambda_{sq} i_{sd}\right) \quad (5)$$

where T_e and p are the electromagnetic torque and pole pairs. The derivative of current in rotor reference frame can be obtained according to (1)-(4) as

$$\frac{d}{dt} i_{sd} = \frac{1}{L_s}\left(-R_s i_{sd} + \omega_r L_s i_{sq} + u_{sd}\right) \quad (6)$$

$$\frac{d}{dt} i_{sq} = \frac{1}{L_s}\left(-R_s i_{sq} - \omega_r L_s i_{sd} - \omega_m \lambda_f + u_{sq}\right) \quad (7)$$

As a result, the stator current derivatives of SPMSG in the rotor frame can be obtained from the machine parameters, rotor speed, permanent magnet flux, currents and the MSC voltage in the d-q frame.

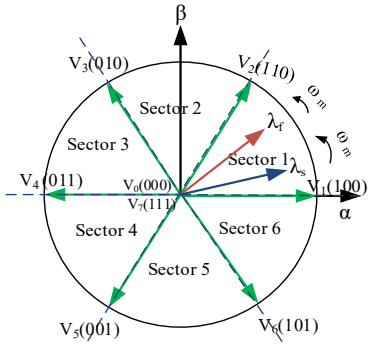

Fig. 2. Eight possible voltage vectors of the MSC.

The MSC can produce eight possible voltage vectors, expressed in the stator reference α–β, according to the state of the six switches. These vectors are shown in Fig.2. In this figure, six sectors are defined by these vectors, and the stator and machine fluxes are shown as an example. Two of these eight vectors are the zero vectors (V_0, V_7) and the rest are the active vectors.

The current slopes in the d-q axis for these eight possible voltage vectors (V_0-V_7) are derived as

$$S_{i_{sd}}\Big|_{u_{sdi}} = \frac{1}{L_s}\left(-R_s i_{sd} + \omega_r L_s i_{sq} + u_{sdi}\right) \quad (8)$$

$$S_{i_{sq}}\Big|_{u_{sqi}} = \frac{1}{L_s}\left(-R_s i_{sq} - \omega_r L_s i_{sd} - \omega_r \lambda_f + u_{sqi}\right) \quad (9)$$

where i and S_i denote the index of the MSC voltage vector and current slope, respectively. The current slopes for these vectors for an 8.7 kW SPMSG along one cycle are shown in Fig. 3. The current slopes for the zero vectors are constant while those for the active vectors are changing sinusoidally.

It is assumed that in the proposed control, four voltage vectors are applied in each switching interval, in which two of them are the zero vectors, and the two remaining vectors are the active vectors. The voltage vector sequence in every period is specified according the corresponding voltage sector. These

vector sequences for each sector are defined in Table. I. The variation of stator current in the d-q frame at the end of a switching interval can be expressed as

$$i_{sd}(k+1) = i_{sd}(k) + S_{da}t_a + S_{db}t_b + S_{dd}t_d \tag{10}$$

$$i_{sq}(k+1) = i_{sq}(k) + S_{qa}t_a + S_{qb}t_b + S_{qd}t_d \tag{11}$$

where S_{da}, S_{db}, S_{dc} and S_{dd} are the current slopes in d axis for the respective voltage vector sequence. S_{qa}, S_{qb}, S_{qc} and S_{qd} represent the current slopes in q axis for the selected vector sequence. The t_a, t_b, t_c, and t_d are the duration times of the corresponding voltage vector sequence.

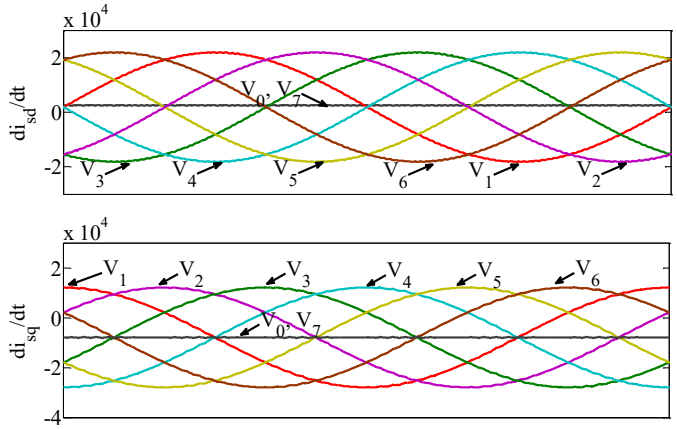

Fig. 3. Current slopes for the voltage vectors: (a) in d axis; (b) in q axis.

TABLE I
VOLTAGE VECTOR SEQUENCES

Vector sequence	Stator voltage Sector (N) 1	2	3	4	5	6
V_a	V_0	V_7	V_0	V_7	V_0	V_7
V_b	V_1	V_2	V_3	V_4	V_5	V_6
V_c	V_2	V_3	V_4	V_5	V_6	V_1
V_d	V_7	V_0	V_7	V_0	V_7	V_0

In order to minimize the error between the current and the reference value in the rotor frame, the well-known cost function is used as follows [5]

$$F(k+1) = \left(i_{sq}(k+1) - i_{sq}^*(k)\right)^2 + \left(i_{sd}(k+1) - i_{sd}^*(k)\right)^2 \tag{12}$$

The duration time of each vector in an interval can be obtained by minimizing the cost function, which yields to

$$t_b = \frac{\left(i_{sd}(k)-i_{sd}^*(k)\right)\cdot(S_{qc}-S_{qa})+\left(i_{sq}(k)-i_{sq}^*(k)\right)\cdot(S_{da}-S_{dc})}{S_{qa}(S_{db}-S_{dc})+S_{qb}(S_{dc}-S_{da})+S_{qc}(S_{da}-S_{db})} + \frac{T_{sw}(S_{qc}\cdot S_{da}-S_{qa}\cdot S_{dc})}{S_{qa}(S_{db}-S_{dc})+S_{qb}(S_{dc}-S_{da})+S_{qc}(S_{da}-S_{db})} \tag{13}$$

$$t_c = \frac{\left(i_{sd}(k)-i_{sd}^*(k)\right)\cdot(S_{qa}-S_{qb})+\left(i_{sq}(k)-i_{sq}^*(k)\right)\cdot(S_{db}-S_{da})}{S_{qa}(S_{db}-S_{dc})+S_{qb}(S_{dc}-S_{da})+S_{qc}(S_{da}-S_{db})} + \frac{T_{sw}(S_{qa}\cdot S_{db}-S_{qb}\cdot S_{da})}{S_{qa}(S_{db}-S_{dc})+S_{qb}(S_{dc}-S_{da})+S_{qc}(S_{da}-S_{db})} \tag{14}$$

$$t_a = t_d = \frac{T_{sw}-t_b-t_c}{2} \tag{15}$$

where T_{sw} is the switching interval. If the estimated durations of active vectors are positive, and the total value $(t_b + t_c)$ is bigger than the switching interval, the duration times should be set to

$$t_b' = \frac{t_b}{t_b+t_c}T_s \tag{16}$$

$$t_c' = \frac{t_c}{t_b+t_c}T_s \tag{17}$$

$$t_d' = t_a' = 0 \tag{18}$$

This case can occur when the stator voltage reference is bigger than the voltage that can be produce by the MSC. When the voltage vector sequence and their durations are calculated, they will be applied like in the space vector modulation (SVM).

B. Sector identification algorithm

In predictive controls, selecting the appropriate voltage sequence is the vital part of the strategy. In many research papers, it has been reported that certain durations of selected active vectors get negative, and the easiest solution was to remove that voltage vector from the switching interval [23]-[25]. This solution makes the switching frequency variable and increases the ripple. To overcome this problem, many predictive controls suggest using two vectors, which consist of one zero vector and one active vector. The active vector of these predictive controls is achieved from the conventional one voltage based predictive controls [26].

These negative values of the duration times occur when the sector that proposes the voltage vector sequence is not selected correctly. In this part, the negative values of the vector durations are investigated, and a stator voltage sector identification algorithm is proposed for the SPMSG.

In Fig. 4, the duration times of the active vectors for the six possible voltage vector sequences during one complete rotation cycle are shown. It can be seen that in each sector, the duration times of the corresponding active vectors are both positive, while in other situations, at least one of the active vectors is negative. For instance, the durations of the V_1 and V_2 are positive only when they are applied in sector 1, or durations of V_2 and V_3 are positive only when they are applied in sector 2. However, in other sectors, if these voltage vectors are chosen, the duration time of one of the vectors is negative at least. For example, as shown in Fig. 4a, the durations of V_1 gets negative in sector 2 if V_1 and V_2 are chosen as the two selected active vectors.

When the duration times of the selected voltage vector sequence get negative, some information can be obtained from this situation that can help to identify the correct sector. When

observing the six cases shown in Fig. 4, these negative duration times can be classified as three types:

1) $t_b < 0$ and $t_c > 0$

When the first active vector duration presents a negative value and the second active vector has a positive value, this indicates that the correct stator voltage sector is one or two sectors ahead. To give an example, assume that the stator voltage is located in sector 2, the V_2 and V_3 are the correct vectors. In this sector, if the V_6 and V_1 are selected, the duration of the V_6 presents a negative value while the V_1 obtains a positive value according to Fig.4f. If duration times of V_1 and V_2 are calculated for sector 2, the duration time of the first active vector will have negative value, and the second vector will be positive, as can be observed from Fig. 4a.

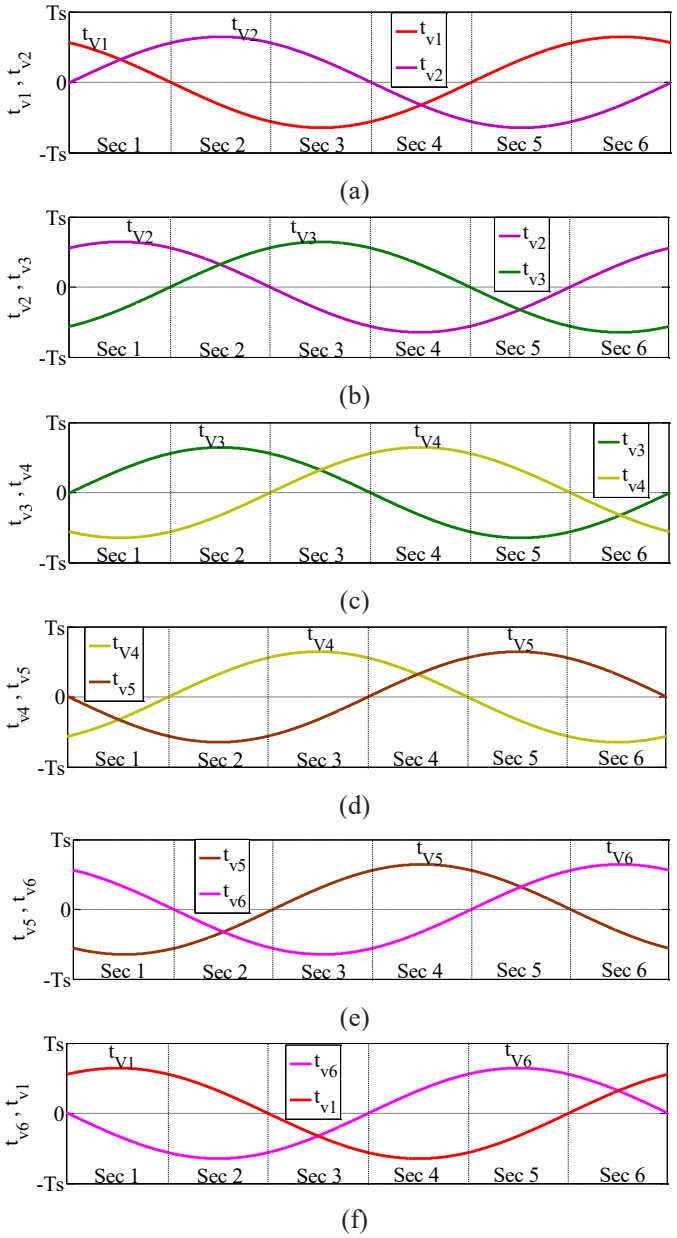

Fig. 4. Active vector durations in one complete rotation cycle: (a) t_{v1}, t_{v2}; (b) t_{v2}, t_{v3}; (c) t_{v3}, t_{v4}; (d) t_{v4}, t_{v5}; (e) t_{v5}, t_{v6}; (f) t_{v6}, t_{v1}.

2) $t_b > 0$ and $t_c < 0$

When the second active vector duration comes to have a negative value and the first active vector has a positive value, this shows that the correct stator voltage sector is one or two sectors behind. For example, if the stator voltage is located in sector 2 and the V_3 and V_4 are selected, the t_{v3} and t_{v4} will be positive and negative, respectively, according to Fig. 4c. On the other hand, according to Fig. 4d, if duration times of V_4 and V_5 are selected in this situation, the second active vector will have a negative value, and the first one will be positive.

3) $t_b < 0$ and $t_c < 0$

The correct stator voltage sector is located exactly three sectors ahead from the initial assumed sector, when both durations become negative. For instance, if the duration times of V_1 and V_2 are calculated when the required stator voltage is located in sector 4, both of the times will have negative values like it is shown in Fig. 4a. This reveals that the correct vectors are V_4 and V_5 and the required stator voltage is located in sector 4.

Consequently, if the durations of the selected active vectors get negative, the sector should be changed according to the respective case type.

C. Overall proposed MPDCC for SPMSG

The block diagram of the proposed predictive control is illustrated in Fig. 5. In each control interval, the voltage vector sequence is chosen according to the previous estimation of the stator voltage sector in the previous interval. The current slopes in the d-q frame for this vector sequence are evaluated from the speed, the permanent magnet flux of the machine and the currents. After that, the durations of the vector sequences are obtained according to these slopes and the measured currents and their references in the d-q frame. If the times of the active vectors are positive, this vector sequence is applied by the electronic converter.

However, one or two of the active vector durations could become negative and, in that case, the sector location should be modified according to the proposed sector identification algorithm. Hence, new voltage vector sequence will be selected, and the duration times of these vectors will be determined. If at the first place, both vector duration times are negative, the sector will be changed to three forward sectors, making the duration times for the new vectors become positive, and so the new vectors will be applied by the converter. However, if only one of the active vector times is negative at the first place, the sector changes to one sector forward or one sector backward depending which duration time got negative. Nonetheless, these new vector durations might get negative again. If they get negative again, this makes obvious that the correct sector is located in two sectors ahead or two sectors behind the first sector assumption. In other words, in the worst case the durations can be calculated three times and in the last time, the duration times of the active vectors will be positive indubitably. This last case could happen when a big sudden change in the position of the stator voltage is required. Finally, after the

correct vector sequences are estimated, the vectors will be applied by the electronic converter.

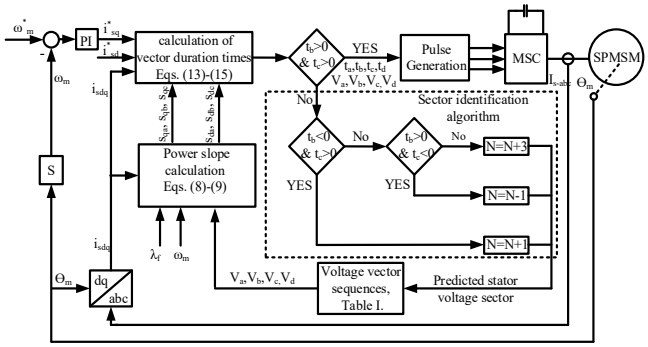

Fig. 5. Block diagram of the proposed MPDCC for SPMSG.

III. OWC BASED POWER PLANT EMULATOR

One of the most well-known wave energy converters is the one based on an oscillating water column (OWC) normally installed onshore, preferably on rocky shores. This type of converter comprises a chamber where the wave is captured, and an air turbine, normally a Wells turbine, that features constant direction of rotation for both direction of the air flow through its blades [27-29]. The schematic of this OWC power plant was shown in Fig. 1.

Waves enter into the OWC chamber forcing the air upwards and downwards, making the Wells turbine to spin and converting wave energy into mechanical energy. Then, the turbine shaft drives an electric generator that converts the mechanical energy into electrical energy.

The strategy chosen in this paper is to make the OWC power plant work at the maximum efficiency point through the control of the rotary speed of the Wells turbine and the electric generator. The highly variable shaft speed is controlled using the proposed MPDCC developed in this paper.

The OWC device behavior has been reproduced using the following mathematical models:

1) Irregular wave model

The irregular wave model represents the state of the free surface of the sea by its energy spectrum, S(ω). This spectrum is obtained from oceanographic buoys measurements and it provides information about the energy content for the frequencies that compose the real wave. The S(ω) can also be used to reproduce the sea state keeping the same spectral characteristics (significant height, peak period, etc.) as the original real waves.

There are many spectra that describe the state of the sea where the OWC is located: Pierson-Moskowitz [30-33], JONSWAP [27-29], [34], TMA [30, 35], and Bretschneider [36].

Using the wave spectrum, S(ω) provided by these models, it is possible to generate an irregular wave represented by the addition of n regular waves, according to the expression

$$\eta(x,t) = \sum_{i=1}^{n} \zeta_i \cdot cos(\omega_i t - k_i x + \varepsilon_i) \quad (19)$$

where the amplitude of each harmonic is:

$$\zeta_i = \sqrt{2 \cdot S(\omega_i) \cdot \Delta\omega_i} \quad (20)$$

Every wave presents a randomly calculated phase and all the phases have the same probability of occurrence, expressed by a constant probability density in the interval (–π, π).

The Pierson-Moskowitz [33] model was chosen in this paper

$$S(\omega) = \frac{5}{16} \cdot H_s^2 \cdot \omega_p^4 \cdot \omega^{-5} exp\left[-\frac{5}{4} \cdot \left(\frac{\omega}{\omega_p}\right)^{-4}\right] \quad (21)$$

where ω = 2π/T is the angular frequency of the wave, H_S is the significant wave height, T_S is the significant wave period and $\omega_p = 2\pi/T_p$ is the angular spectral peak frequency. Fig. 6 shows the real wave profile generated for the tests carried out in this paper.

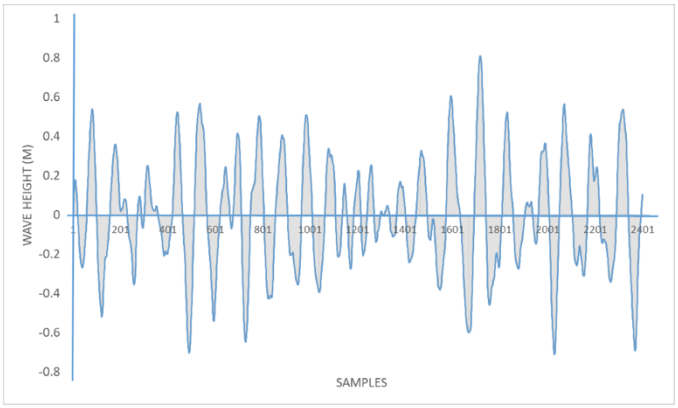

Fig. 6: The real wave profile used in this paper is made up of 2400 samples H_s=1 and T_s=10.

2) Chamber model

Detailed modeling of the chamber in an OWC device, results in complex mathematical models [37-39]. The OWC device equations programed in the emulator represent a simplified chamber model [17]. As a consequence, the hydrodynamics inside the chamber is not fully described, but what it is more relevant from the electrical point of view, the electrical power delivered to the grid does not lose the multi frequency spectrum of the wave resource.

The air speed in the duct of the turbine can be described by the following expression (see Table A1 and Table A2 in Appendix for the nomenclature, and Table A3 for the turbine parameters):

$$V_x = \left(\frac{A_c}{A_d}\right) \cdot \frac{\partial h_c}{\partial t} \quad (22)$$

The torque coefficient, C_t, depends on the characteristic curve of each particular turbine and is a function of the air flow through the turbine, Φ:

$$\Phi = \frac{V_x}{r_t \cdot \omega_t} \quad (23)$$

3) Wells turbine torque emulation

The Wells turbine torque can be obtained as

$$T_t = C_t \cdot K \cdot Radius \cdot [V_x^2 + (Radius \cdot \omega_t)^2] \quad (24)$$

Fig. 7 shows, in solid line, the characteristic curve (Ct - Φ) of the turbine model that has been represented in the prototype [18][40] and the efficiency curve in dashed line.

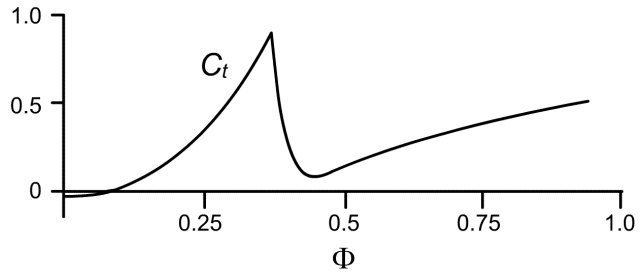

Fig. 7. C_t as a function of the flow coefficient. The graph is symmetrical with respect to the 'y' axis for negative values of Φ.

For every wave and V_x, the calculated Wells turbine torque is reproduced using a separately excited DC motor, Fig. 8. However, for every calculated motor torque, the resulting rotary speed depends also on the opposite torque. At this point is where the proposed MPDCC method system performance becomes very important since it controls the opposite torque created by the SPMSG to make the power plant to work at the maximum efficiency point in every moment.

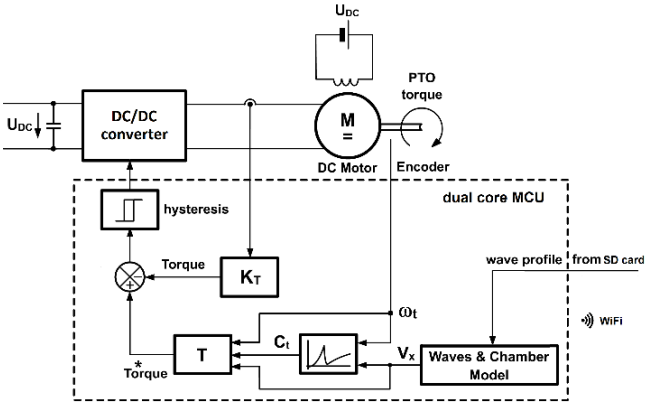

Fig. 8. Control block of the OWC device emulator.

The torque control of the SPMSG uses the Φ for the maximum efficiency obtained from Fig. 7. For this given Φ, the corresponding rotary speed, ω_t is calculated for every wave and V_x in every control cycle and used as reference speed in the proposed MPDCC control system, Fig. 5.

4) Maximum efficiency speed reference for the MPDCC

The speed reference used by the MPDCC block, Fig. 5, is the Wells turbine maximum efficiency speed. This speed is calculated according to the maximum efficiency flow coefficient represented in the turbine efficiency curve [40][41], Fig. 9.

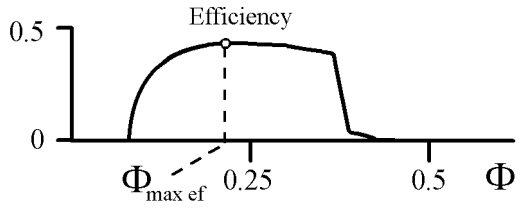

Fig. 9. Wells turbine efficiency as a function of the flow coefficient.

In every program cycle, the microcontroller calculates the airspeed from the wave height inside the chamber, (22). Then, using the $\Phi_{max\ ef}$ obtained from Fig .9, and the turbine radius, the maximum efficiency speed is calculated by using (23). The block diagram of Fig .10 shows this procedure.

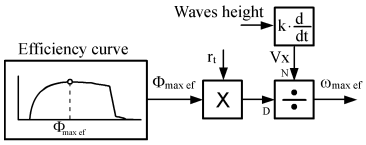

Fig. 10. Calculation of the maximum efficiency speed.

IV. Simulation Results

The proposed MPDCC for SPMSG is evaluated using Matlab/Simulink, and the simulation results are presented throughout this section. The selected switching frequency and the sampling frequency, both were 4 kHz. Firstly, the dynamic performance and current THD of the proposed MPDCC are checked and compared with conventional one voltage vector MPC [5] and two voltage vectors MPC [9]. Secondly, the performance of the proposed control is assessed in the described OWC power plant emulator using a real wave profile. The machine parameters of the simulated system and the laboratory setup are displayed in Table II.

In dynamic performance study, the generator speed was accelerated from 0 at t=1s to the rated speed in 0.5 seconds. The references of d and q axis stator currents were set to 0A and -8A at the beginning of the simulation. However, at t=1.2 s, the i^*_{sq} was set to -4 A, and i^*_{sd} was changed to 1 A at t=1.3s. The simulation results of this study for the proposed MPDCC, the conventional one voltage vector MPC and two voltage vectors MPC methods are shown in Fig. 11, Fig. 12 and Fig. 13, respectively. All the predictive controls follow the current references correctly and have a fast dynamic response to the sudden changes in the references. However, it is very clear in these figures that the proposed MPDCC has a lower ripple in d-q currents, the torque and the stator flux. Moreover, the stator current for the proposed MPDCC "is cleaner" and sinusoidal. In the proposed MPDCC, the duration times of the active vectors are increased when the generator speed is high, as can be seen in Fig. 11g. This is because, at low speeds, the zero vectors have small current slopes. Therefore, in most portions of the period, these vectors are employed in order to minimize the current ripples.

The stator voltage sector and the durations of the active vectors for the proposed control are illustrated in Fig. 11f and Fig. 11g, respectively. It can be observed that the duration times of all of the active vectors are positive, which demonstrate that

the proposed sector identification algorithm works very well and can find the correct voltage vector sequences quickly.

TABLE II
SPMSG PARAMETERS

DC Link voltage	600 V
Rated power	8.7 kW
Rated voltage	400 V
Number of pole pairs	3
Permanent magnet Flux	1.05 Wb
Stator Inductance	50 mH
Stator resistance	2 Ω

Among the presented MPC strategies, the conventional one voltage vector MPC has higher ripple in all the variables. The performance of the two-voltage vector MPC is better than the conventional one voltage vector MPC. The torque, stator flux and current ripples in the two voltage vectors MPC are lower than in the one voltage vector MPC. The performance of the two-voltage vector MPC at low speeds is good and is similar to the proposed MPDCC since a zero vector is applied in each period. However, during higher speeds, the current ripples of the two-voltage vector MPC is increased significantly while the current ripple for the proposed control is lower.

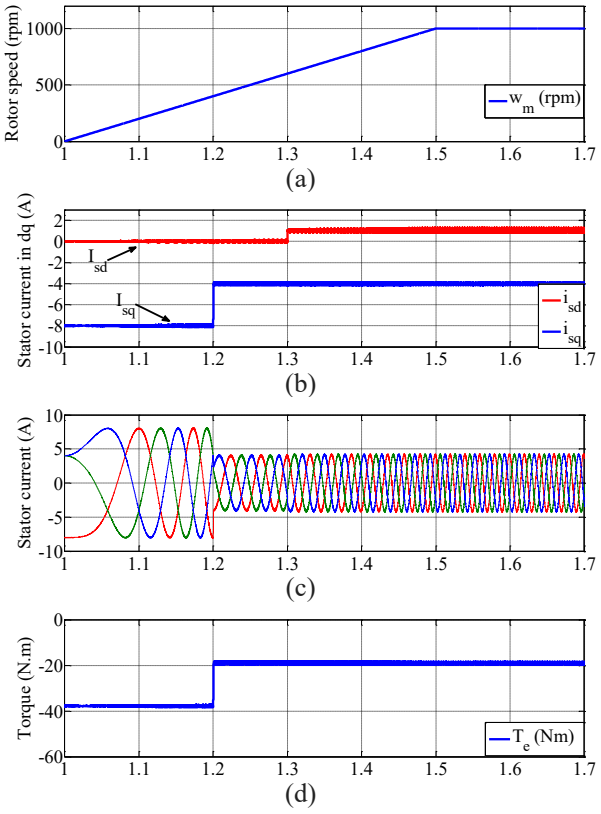

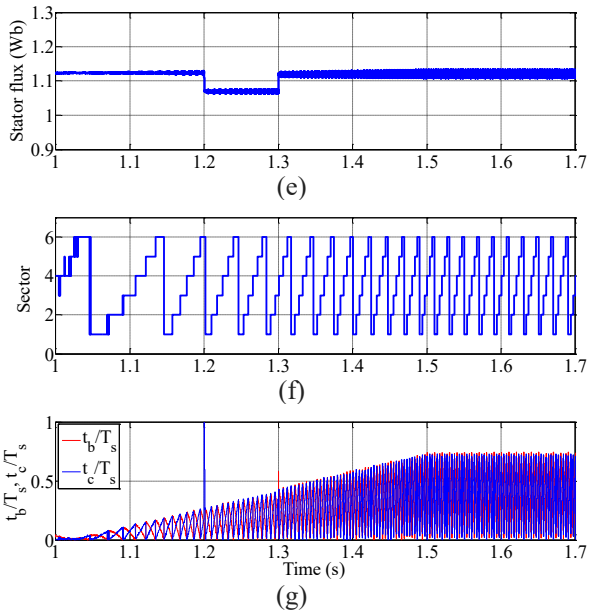

Fig. 11. Simulation results for the Proposed MPDCC for SPMSG: (a) generator speed; (b) stator current in the d-q frame; (c) three-phase stator current; (d) electromagnetic torque; (e) stator flux; (f) sector; (g) active vector durations.

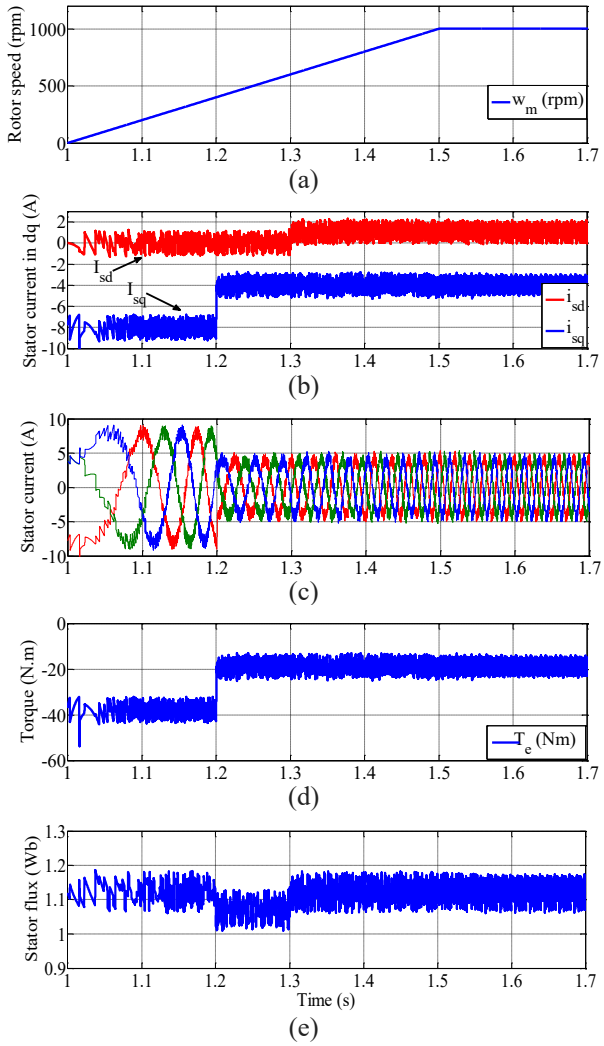

Fig. 12. Simulation results for the conventional one voltage MPC for SPMSG: (a) generator speed; (b) stator current in the d-q frame; (c) three-phase stator current; (d) electromagnetic torque; (e) stator flux.

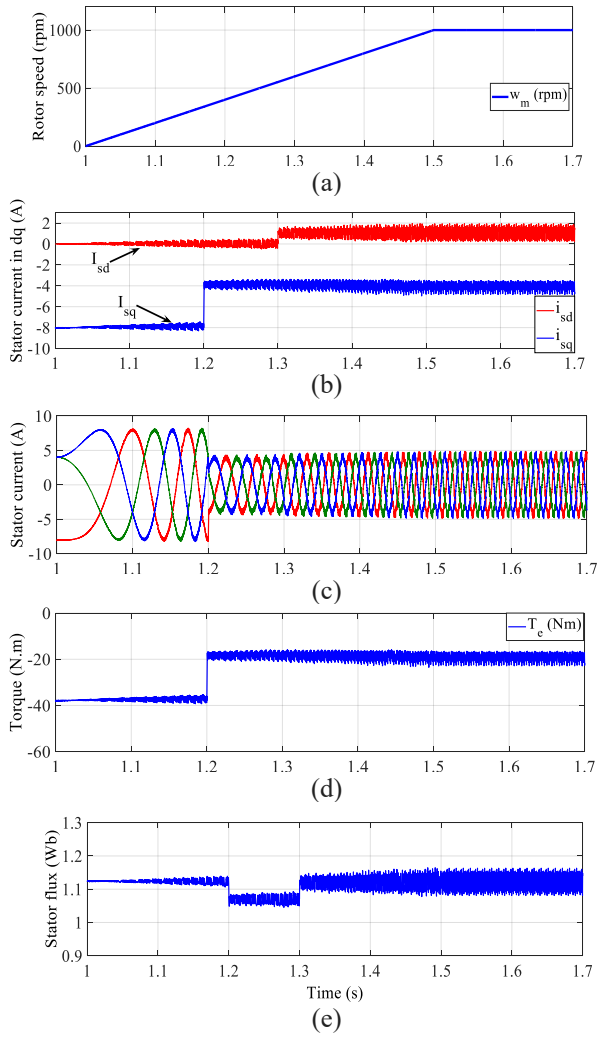

Fig. 13. Simulation results for the two voltage vectors MPC for SPMSG: (a) generator speed; (b) stator current in the d-q frame; (c) three-phase stator current; (d) electromagnetic torque; (e) Stator flux.

In order to compare the harmonic spectrum of the proposed MPDCC with the conventional one voltage vector and two voltage vectors MPC control, FFT analyses were carried out at t=1.62 s for one cycle. One of the current phases and the harmonic spectrum for the proposed MPDCC, conventional one voltage vector MPC and two voltage vectors MPC controls are presented in Fig. 14, Fig. 15 and Fig. 16, respectively. The total harmonic distortion (THD) of the stator current for the proposed MPDCC is 2.63%, which is much lower than the conventional one voltage vector and two voltage vectors MPC with THD values of 16.06% and 10.23%, respectively.

The results for the conventional MPC show that the stator current contains high low-order harmonics, in consequence, they are difficult to remove by means of filters. In two voltage vectors MPC the low-order harmonics are decreased compared to the conventional MPC. However, still these harmonics are notable. In contrast, for the proposed MPDCC, the dominant harmonics are located around the 4 kHz and 8 kHz and so on.

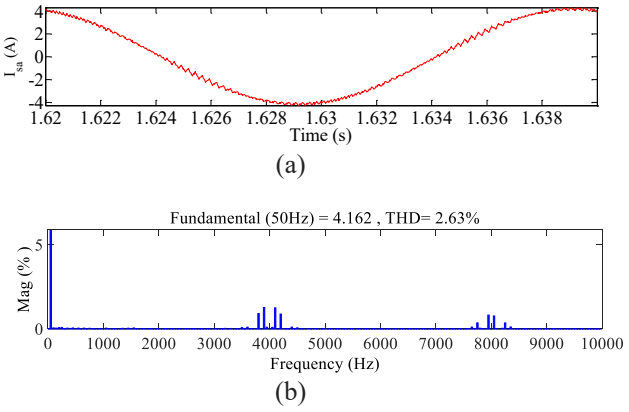

Fig. 14. Harmonic spectrum of proposed MPDCC for SPMSG in simulation at t=1.62 s: (a) phase “a” current; (b) Harmonic spectrum.

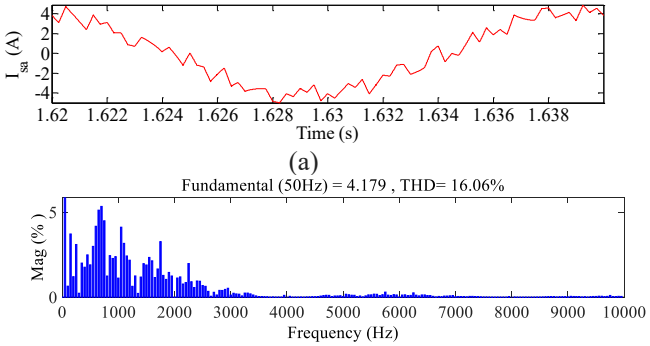

Fig. 15. Harmonic spectrum of conventional one voltage vector MPC for SPMSG in simulation at t=1.62 s: (a) Phase “a” current; (b) Harmonic spectrum.

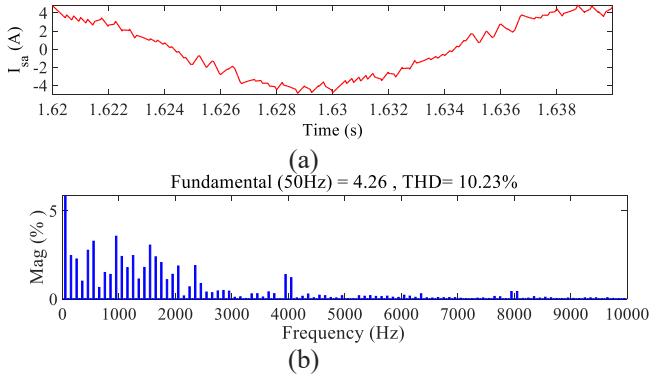

Fig. 16. Harmonic spectrum of two vectors MPC for SPMSG in simulation at t=1.62 s: (a) Phase “a” current; (b) Harmonic spectrum.

However, even using the same control period for the three cases, the switching frequency of the one voltage vector and the two voltage vector MPCs are both variable and their average switching frequencies are lower than that of the proposed MPDCC.

In order to check the robustness of the proposed MPDCC method to the parameter variations, it has been assumed, as an example, that the stator inductance is 30% lower than its real value. The same study conditions of Fig. 11 were set to check the change in the performance due to the inductance variation. The resulting stator current in dq frame is shown in Fig. 17. As can be seen, the proposed method makes the current dq components to follow the references accurately. Moreover, an FFT analysis was carried out at t=1.62 s to check the stator current THD and to compare it with that of Fig. 14. The stator current THD for this case is shown in Fig. 18. As can be seen, the current THD value for this case is almost the same as when the real value is used.

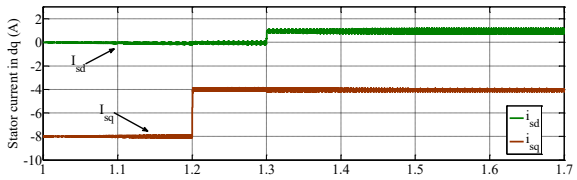

Fig. 17. Stator current in dq frame for the proposed MPC control with 30% of stator inductance error.

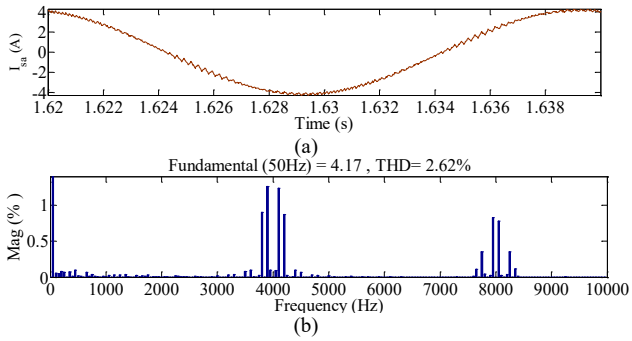

Fig. 18. Harmonic spectrum of proposed MPDCC for SPMSG during the 30% stator inductance error in simulation at t=1.62 s: (a) phase "a" current; (b) Harmonic spectrum.

Moreover, the proposed MPDCC has been tested in OWC power plant for 45 seconds using an irregular wave. The test was done for the wave profile shown in Fig. 6 and for the first 450 samples. In this test i^*_{sd} was set to zero. The results are illustrated in Fig. 19. The Wells turbine maximum efficiency speed and the actual speed during the 45 seconds test are shown in Fig. 19.a with blue and red lines, respectively. As can be seen, with the proposed control, the generator follows the maximum efficiency speed perfectly during the test. The d axis, q axis and three-phase stator current are shown in Fig. 19b, Fig. 19c and Fig. 19d, respectively. The stator current in q axis varies in order to make the Wells turbine to work at the maximum efficiency point.

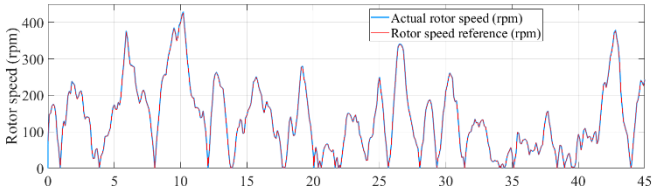

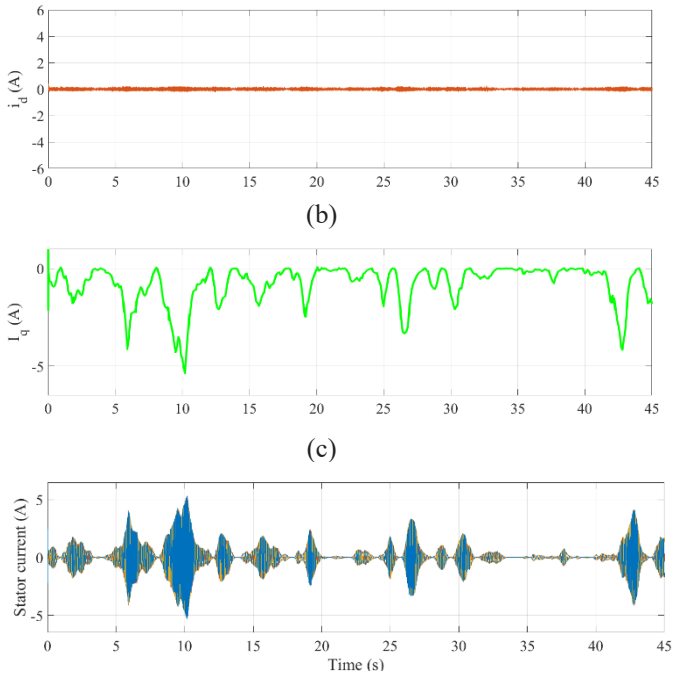

Fig. 19. Simulation results for 45 seconds of OWC test: (a) Rotor speed (speed reference (blue line) and actual speed (red line)) (b) stator current in d axis (c) stator current in q axis (d) stator current in abc frame.

A more detailed view of this test during t=10 s to t=12 s is presented in Fig. 20. It can be seen that the proposed control strategy follows the maximum efficiency reference speed with good accuracy, and the stator currents are sinusoidal and balanced during this test.

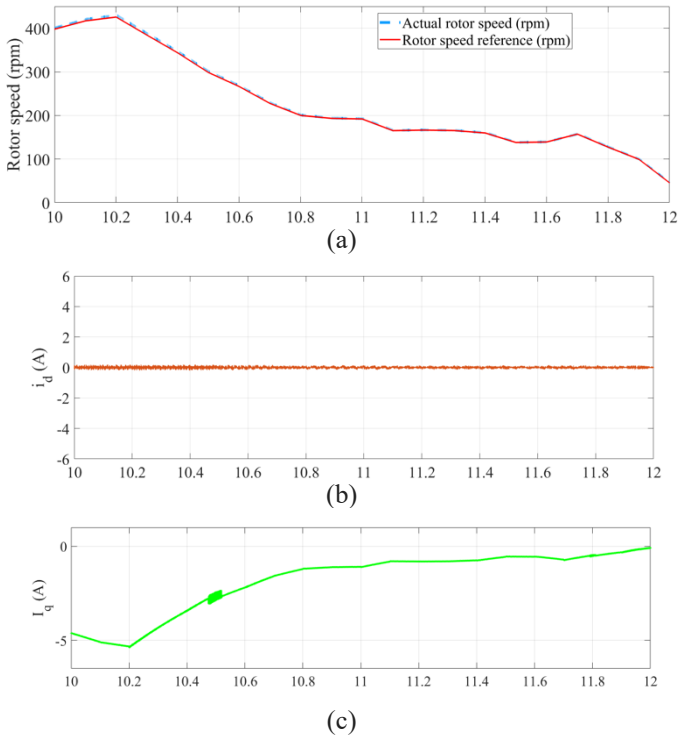

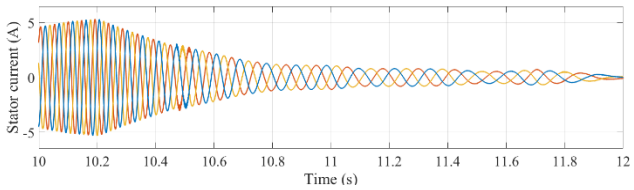

(d)

Fig. 20. Detailed view of the simulation results of the OWC during t=10s to t=12s: (a) Rotor speed (speed reference (dash blue line) and actual speed (red line)) (b) stator current in d axis (c) stator current in q axis (d) stator current in abc frame.

V. Experimental Results

As aforementioned in section I, WECs are subject to variations of torque and speed generated by the incoming and outgoing waves. Depending on the sea state, these variations can be sudden and large in amplitude and persistent over time when the sea is rough, or very low when the sea is calm. For this reason, a maximum efficiency-based control of the WEC should provide a precise torque control over a wide range of speed and torque.

Firstly, the laboratory prototype is described. Secondly, the dynamic performance of the proposed MPDCC is evaluated in a laboratory experimental setup during different transient tests and later the results obtained from several experimental tests carried out in the laboratory using a SPMSG in a WEC emulator are presented. The objective of testing the proposed control in a WEC emulator was to verify the ability of the proposed MPDCC to satisfy the high torque requirements of an OWC based power plant.

A. Description of the laboratory prototype

The prototype of the power plant is divided into two different systems: the "OWC device" and the "Electric power generation system". Fig. 21 shows the layout of both parts, along with an external electric power system to which the prototype is connected, and that absorbs the generated electrical power. A photo of the experimental prototype is shown in Fig. 22.

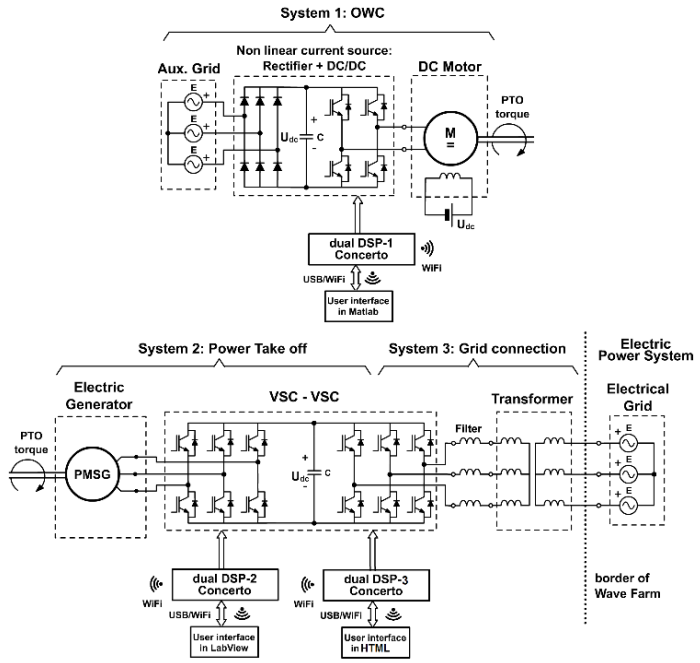

Fig. 21. Schematic of the test bench used to carry out the experimental tests.

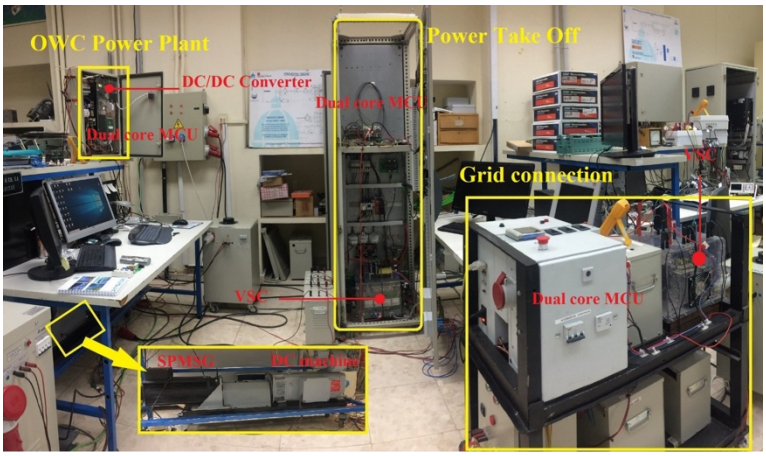

Fig. 22. Overview of the experimental test bench.

1) OWC device

The prototype part that simulates the OWC device, system 1 in Fig. 21, reproduces: the irregular wave, the chamber containing the oscillating water column, and the Wells turbine.

From the irregular wave profile, the control program calculates, in each cycle, the corresponding turbine torque by means of the chamber and the Wells turbine models. Then, this torque is reproduced in real time using a separately excited DC motor. The sea state used in the OWC emulator was characterized by a significant wave height $H_s = 1m$ and an energy period $T_e = 10s$ and the wave profile was generated using the Pierson-Moskowitz model [30],[32].

2) PTO and grid connection

The second part of the prototype, system 2 and system 3 in Fig. 21, reproduces the entire electrical system of the OWC power plant and the grid connection using real elements. As

Fig. 22 shows, a SPMSG connected to the DC motor shaft (Wells turbine shaft) and a three-phase converter represent the PTO, which is controlled by the proposed MPDCC, while the grid connection is carried out using a vector-controlled three phase converter.

The dual core microcontroller used to program the MPDCC code was a F28M35x Concerto of Texas Instruments with a switching frequency of 4kHz and a sampling time of 250µs. All of the waveforms were recorded using the F28M35x itself, except the stator currents, that were recorded using a Tektronix TDS2024C oscilloscope with a sampling time of 100µs. The computation burden for the proposed control in F28M35x is 122 µs, while for the conventional one voltage vector MPC and two voltage vectors MPC is 95.5 µs and 100 µs, respectively. This indicates that the calculation burden of the proposed method is not high if compared to the two other MPC methods.

B. Dynamic performance of the proposed control

First of all, the electric current waveform quality was checked for several torque levels. Fig. 24 shows the generator phase currents corresponding to two different torque levels while rotor speed is around 205 rpm. In both, the waveform is almost ripple-free and is balanced.

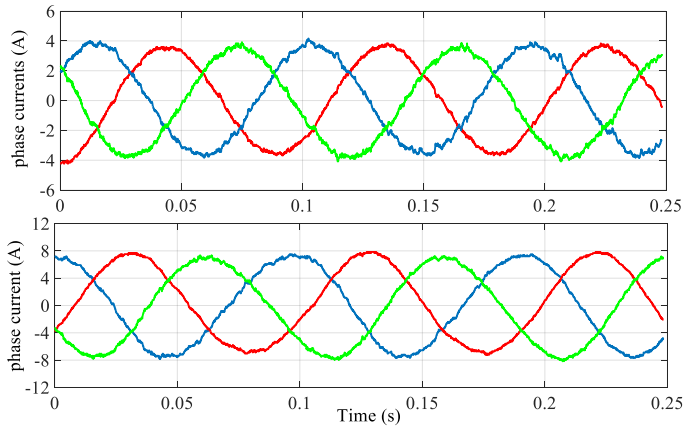

Fig. 23. Stator currents when i_{sq} reference was set to -4A (top) and to -8A (bottom) whereas the i_{sd} reference was set to zero in both cases.

The harmonic spectrum corresponding to the stator current of Fig. 23 bottom, is shown in Fig. 24. The resulting THD calculated up to 2 kHz is 4.16% which is reasonably low taking into account that the stator emf is not completely sinusoidal and the rotor speed (frequency) is not completely constant.

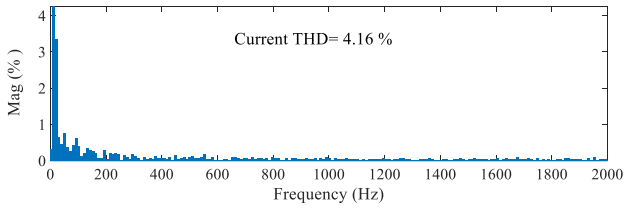

Fig. 24. Stator current THD. The fundamental frequency is 10.22Hz and its magnitude is 7.81.

Secondly, the proposed control was assessed when the rotor speed increases. In this case, the rotor speed was increased from 250 rpm to 750 rpm and the d and q axis stator current references were set to 0A and -4A, respectively. The three-phase stator current and the rotor speed are displayed in Fig. 25. The stator current of this test was acquired (registered) by the DSP every 2 ms. The stator current frequency increased and followed the references when the rotor speed was increased.

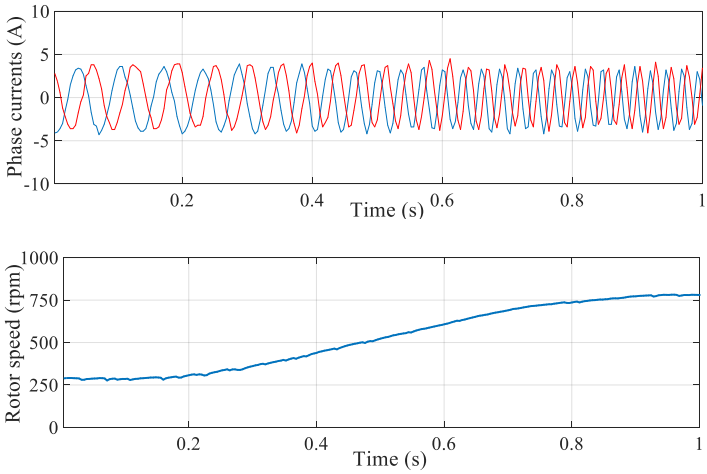

Fig. 25. Stator currents and rotor speed during a rotor speed increment test.

Thirdly, the performance of the proposed control was tested using a reference torque step and a reference field step. It must be taken into account that the usual dynamic of a WEC might change within the range between several tenths of seconds to several seconds, not in the order of milliseconds. Fig. 26 shows the fast response of the actual i_{sq} following its reference during a step, from -4A to -6A, while the SPMSG generates active power. The order of the time response indicates that this control is suitable to cope with the WECs dynamics. As can be seen, the stator current is sinusoidal and balanced during the test.

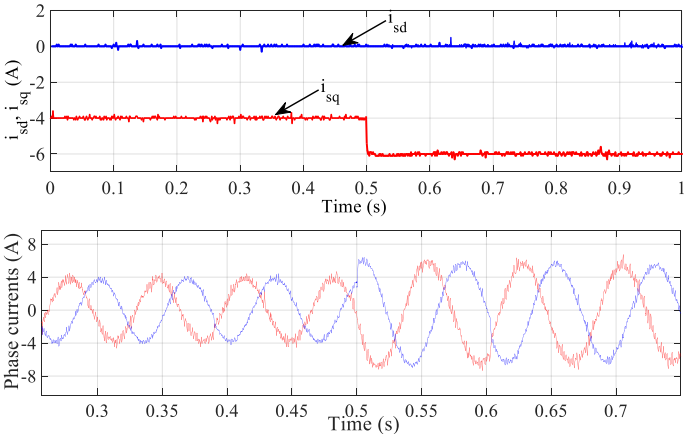

Fig. 26. Torque control of the SPMSG through i_{sq}. Step response when reference changes from -4A to -6A. Note how fast the actual i_{sq} tracks the new reference after the step. The i_{sd} reference was set to zero.

The following test checked the proposed predictive control ability to control the magnetic field in the electric generator, what is of paramount importance to obtain a good toque control.

Although the magnetic field has a slow dynamic response, Fig. 27 shows how the MPDCC is able to get the new i_{sd} reference in a very short time. In this case, a field weakening was carried out, taking into account not to reach the irreversible demagnetizing point. The magnetic field weakening would allow to increase the rotary speed of the generator surpassing the rated speed in the event of a sudden large wave.

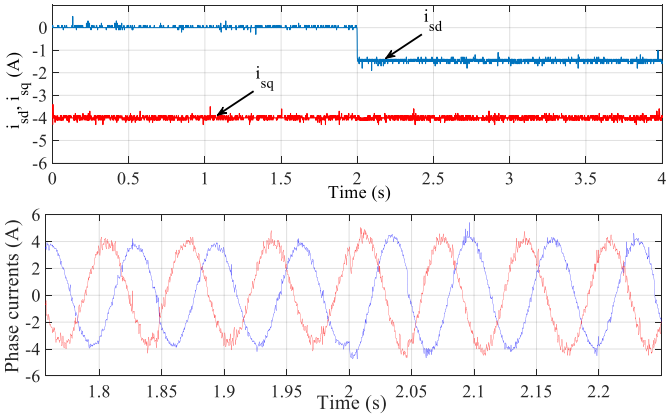

Fig. 27. Magnetic field control of the SPMSG through i_{sd}. Step response of the actual i_{sd} when the reference changes for 0A to -1.5A, carrying out a magnetic field weakening. i_{sq} reference was set to -4 A.

C. *OWC power plant performance*

Once the dynamic performances of the MPDCC were checked, the next step was to implement the control in an OWC-based power plant. In this control, the generator shaft speed is taken to the maximum efficiency point through the torque control.

As the incoming and outgoing waves push the air flow through the chamber, it makes the turbine and generator to rotate with changing speed. Fig. 28 shows the magnetic field angle and the electromotive force angle registered in the generator from the starting point when the irregular wave profile is used with the OWC emulator. Note the 90º diphase existing between them and the large rotary speed variations.

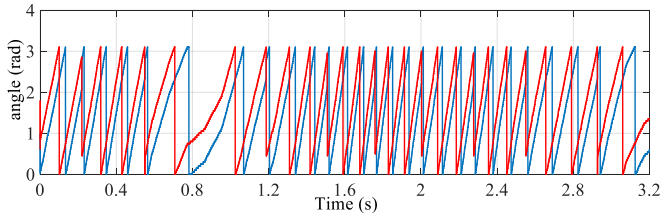

Fig. 28. Magnetic field angle (blue) and electromotive force angle (red) at the starting point of the test.

The wide range of speed variation makes the control of the generator more difficult. On the one hand, an accurate speed and shaft position measurement over the whole range, even close to zero rpm, becomes complex. So, the MPDCC should be robust to inaccuracies. Also, close to zero speed implies a negligible electromotive force in the generator, what makes the stator current change very fast as the voltage pulses are applied by the VSC. However, as the tests below will show, the robustness and fast dynamic of the proposed MPDCC make the control handle these problems properly.

In the following tests, an irregular wave profile was used in the OWC emulator. This irregular wave leads to a changing maximum efficiency speed which must be tracked by the torque control whereas the field control maintains the magnetic field constant.

Fig. 29 shows the reference speed needed to get the maximum efficiency (blue) and the actual shaft speed (red) along the test that obtained in a 4 minutes long test, where the rotary speed follows the speed reference very accurately along the whole test. Note the large speed variations and the irregular speed profile within this test.

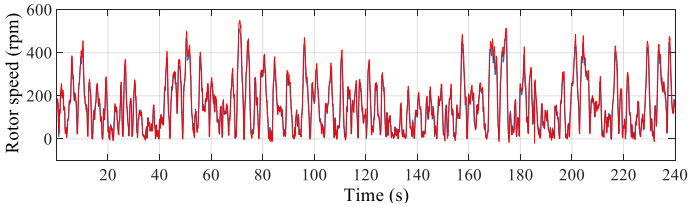

Fig. 29. Rotary speed reference (blue) vs. actual speed (red) during a 4 minutes long test.

Fig. 30 shows a more detailed view of reference and actual speeds from t=20 s to t=80 s. As can be seen the rotor speed is following the reference value with a small error in some points.

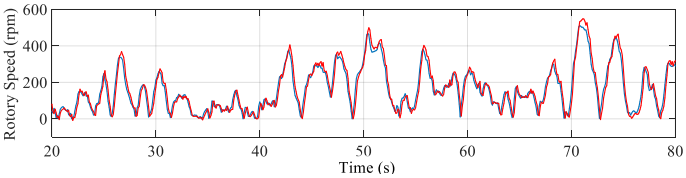

Fig. 30. Detailed view of the rotary speed reference (blue) and actual rotary speed (red) during the test.

The actual torque is a fast-changing magnitude, so the torque control has to follow a fast reference given by the q component of the stator current. Fig. 31 shows the large changes appearing in the i_{sq} reference and how the actual i_{sq} (red) follows the reference (blue) very accurately meaning that the PTO works approximately at the maximum efficiency at any time.

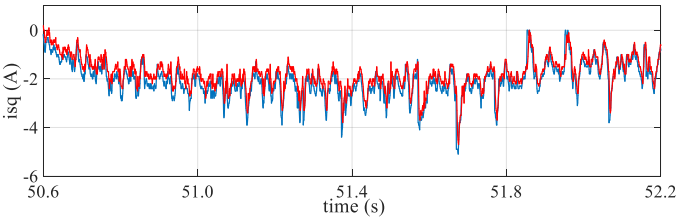

Fig. 31. The torque control generates fast changing reference for i_{sq} while for i_{sd} keeps constant. A detailed view, sampled by the DSP each 0.00250 s, shows the actual i_{sq} and i_{sd} following their references accurately at every moment.

VI. Conclusions

Wave energy is a promising energy source still under development. Its special characteristics make this technology go ahead slowly. While it is more foreseeable and less stochastic than wind energy for example, the hardness of the sea

environment and the lack of a predominant technology, make it difficult to get prototypes to a commercial stage.

One of the problems to be addressed is the development of specific control techniques designed to extract the maximum amount of energy from the sea. A specific problem of wave energy conversion is the sudden and large variations of torque and speed the WECs are subjected to. This paper presents a fast and robust torque control, based on a MPDCC, able to deal with these variations.

The proposed MPDCC is easy to implement in a microcontroller and its computing time means not a bigger burden than the amount of time typically spent in a classical vector control. Results show that the MPDCC can effectively predict the appropriate sector and voltage vector sequences while keeping the switching frequency fixed as well.

When it is used with SPMSGs, only one PI regulator is needed so the magnetic field and torque control carried out by means of the predictive calculation of the d-q components of the stator current are very fast whereas the ripple in the stator currents is very low.

The simulation results revealed that the proposed MPDCC has a significant performance compared to conventional one voltage vector and two-voltage vector MPC methods. Moreover, electric currents present a low current THD and the rest of variables a low ripple.

The experimental tests carried out using a wave energy power plant emulator show how the MPDCC is able to make the rotary speed follow the reference although it changes in a wide range and in a very irregular manner. Therefore, it can be said that the proposed MPDCC presents a suitable behavior to control a SPMSG in wave energy conversion.

APPENDIX: NOMENCLATURE

TABLE A1. Chamber model.

V_x	Air speed in the duct (m/s)
h_c	Height of the free water surface inside the chamber (m)
A_c	Chamber cross section (m^2)
A_d	Duct cross section (m^2)

TABLE A2. Turbine model

T_t	Shaft torque (N.m)	r_t	Turbine radius (m).
ϕ	Flow coefficient (non-dimensional)	V_x	Air speed in duct (m/s).
C_t	Torque coefficient (non-dimensional)	ω_t	Angular velocity of rotor system (rad/s)
K	Constant of the turbine (kg/m)		

TABLE A3. Wells Turbine parameters

Maximum efficiency flow $\phi_{max\,ef} = 0.17$	Maximum Ct before stall	for $\phi = 0.311$
	Air density	$\rho = 1.2\ kg/m^2$
	Height of the blades	b=0.045 m
	Blade chord length	l =0.090 m
	Number of turbine blades	n=8

ACKNOWLEDGMENTS

This work has been partially funded by the project DPI2017 - 88505 - C2 -1 -R of the call for R + D + i projects, of the Spanish State Program of Research, Development and Innovation Oriented to the Challenges of Society.

REFERENCES

[1] Jun-Koo Kang and Seung-Ki Sul, "New direct torque control of induction motor for minimum torque ripple and constant switching frequency," in IEEE Transactions on Industry Applications, vol. 35, no. 5, pp. 1076-1082, Sept.-Oct. 1999.

[2] G. S. Buja and M. P. Kazmierkowski, "Direct torque control of PWM inverter-fed AC motors - a survey," in IEEE Transactions on Industrial Electronics, vol. 51, no. 4, pp. 744-757, Aug. 2004.

[3] D. Casadei, F. Profumo, G. Serra, and A. Tani, "FOC and DTC: Two viable schemes for induction motors torque control," IEEE Trans. Power Electron., vol. 17, no. 5, pp. 779–787, Sep. 2002.

[4] Y. Inoue, S. Morimoto, and M. Sanada, "Comparative study of PMSM drive systems based on current control and direct torque control in flux-weakening control region," IEEE Trans. Ind. Appl., vol. 48, no. 6, pp. 2382–2389, Nov. 2012.

[5] J. Rodriguez et al., "Predictive current control of a voltage source inverter," IEEE Trans. Ind. Electron., vol. 54, no. 1, pp. 495–503, Feb. 2007.

[6] F. Morel, X. Lin-Shi, J.-M. Retif, B. Allard, and C. Buttay, "A comparative study of predictive current control schemes for a permanent-magnet synchronous machine drive," IEEE Trans. Ind. Electron., vol. 56, no. 7, pp. 2715–2728, Jul. 2009.

[7] Z. Zhang, J. Rodríguez and R. Kennel, "Advanced control strategies for direct-drive PMSG wind turbine systems: Direct predictive torque control approaches," CPSS Transactions on Power Electronics and Applications, vol. 2, no. 3, pp. 217-225, Sept. 2017.

[8] P. Landsmann and R. Kennel, "Saliency-based sensorless predictive torque control with reduced torque ripple," IEEE Transactions on Power Electronics, vol. 27, no. 10, pp. 4311-4320, Oct. 2012.

[9] Y. Zhang, W. Xie, Z. Li, and Y. Zhang, "Model predictive direct power control of a pwm rectifier with duty cycle optimization," IEEE Transactions on Power Electronics, vol. 28, no. 11, pp. 5343-5351, Nov. 2013.

[10] H.Fang, Z. Zhang, X. Feng, and R. Kennel, "Ripple-reduced mpdpc for active front end power converters with extended switching vectors and time-optimized control," IET Power Electronics, no. 11, p. 22, Apr. 2016.

[11] Z. Zhang and R. Kennel, "Novel ripple reduced direct model predictive control of three-level NPC active front end with reduced computational effort," in Predictive Control of Electrical Drives and Power Electronics (PRECEDE 2015), Valparaiso, Chile., 2015

[12] Z. Zhang, H. Fang, F. Gao, J. Rodrguez, and R. Kennel, "Multiplevector model predictive power control for grid-tied wind turbine system with enhanced steady-state control performance," IEEE Transactions on Industrial Electronics, vol. 64, no. 8, pp. 6287-6298, Aug. 2017.

[13] D. Zhou, P. Tu and Y. Tang, "Multivector Model Predictive Power Control of Three-Phase Rectifiers With Reduced Power Ripples Under Nonideal Grid Conditions," IEEE Transactions on Industrial Electronics, vol. 65, no. 9, pp. 6850-6859, Sept. 2018.

[14] M. E. Zarei, C. Veganzones Nicolás and J. Rodríguez Arribas, "Improved Predictive Direct Power Control of Doubly Fed Induction Generator During Unbalanced Grid Voltage Based on Four Vectors," IEEE Journal of Emerging and Selected Topics in Power Electronics, vol. 5, no. 2, pp. 695-707, June 2017.

[15] T. Geyer, "Computationally efficient model predictive direct torque control," IEEE Transactions on Power Electronics, vol. 26, no. 10, pp. 2804-2816, 2011.

[16] T. Geyer and D. E. Quevedo, "Multistep direct model predictive control for power electronics -Part 2: Analysis," Energy Convers. Congr. Expo. (ECCE), 2013 IEEE, pp. 1162-1169, 2013.

[17] D. Ramirez, J. P. Bartolome, S. Martinez, L. C. Herrero and M. Blanco. Emulation of an OWC ocean energy plant with PMSG and irregular wave model", IEEE Transactions on Sustainable Energy, vol. 6, no. 4, Oct. 2015.

[18] D. Ramirez; G. Venkataramanan. “Development System for Wireless Control applied to Renewable Power Plants”. IEEE Transactions on Sustainable Energy. Volume: PP, Issue: 99, 13 December 2017.
[19] A. F. O. Falcao and P. A. P. Justino, “OWC wave energy devices with air flow control,” Ocean Eng., vol. 26, no. 12, pp. 1275–1295, 1999.
[20] M. Amundarain, M. Alberdi, A. J. Garrido, and I. Garrido. “Modeling and Simulation of Wave Energy Generation Plants: Output Power Control”. IEEE Transactions on Industrial Electronics, vol. 58, no. 1, January 2011.
[21] A M. Alberdi, M. Amundarain, A. J. Garrido, I. Garrido, O. Casquero, and M. De la Sen. “Complementary Control of Oscillating Water Column-Based Wave Energy Conversion Plants to Improve the Instantaneous Power Output”. IEEE Trans. on Energy Conversion, vol. 26, no. 4, December 2011.
[22] N. Mohan, Advanced Electric Drives: Analysis, Control, and Modeling Using Matlab/Simulink. Hoboken, NJ, USA: Wiley, 2014.
[23] G. Abad, M. Á. Rodriguez and J. Poza, "Two-Level VSC Based Predictive Direct Torque Control of the Doubly Fed Induction Machine With Reduced Torque and Flux Ripples at Low Constant Switching Frequency," IEEE Transactions on Power Electronics, vol. 23, no. 3, pp. 1050-1061, May 2008.
[24] G. Abad, M. Á. RodrÍguez and J. Poza, "Two-Level VSC-Based Predictive Direct Power Control of the Doubly Fed Induction Machine with Reduced Power Ripple at Low Constant Switching Frequency," IEEE Transactions on Energy Conversion, vol. 23, no. 2, pp. 570-580, June 2008.
[25] J. Hu and Z. Q. Zhu, "Investigation on Switching Patterns of Direct Power Control Strategies for Grid-Connected DC–AC Converters Based on Power Variation Rates," IEEE Transactions on Power Electronics, vol. 26, no. 12, pp. 3582-3598, Dec. 2011.
[26] Y. Zhang, D. Xu, J. Liu, S. Gao and W. Xu, "Performance Improvement of Model-Predictive Current Control of Permanent Magnet Synchronous Motor Drives," IEEE Transactions on Industry Applications, vol. 53, no. 4, pp. 3683-3695, July-Aug. 2017.
[27] Hasselmann et al. 1973 “Measurements of wind-wave growth and swell decay during the joint North Sea Wave Project (JONSWAP)” Dtsch. Hydrogr Z. Suppl” 12, A8.
[28] Hasselmann, D.E., Dunckel, M. y Ewing, J.A. 1980 “Directional wave spectra observed during JONSWAP 1973” J. Phys. Ocean., 11, 718-728.
[29] Y. Goda. Random seas and design of maritime structures. 3rd edition. World Scientific Publishing Co. ISBN: 978-981-4282-39-0. 2010.
[30] Recommended practice. Det Norske Veritas DNV-RP-C205. Environmental conditions and environmental loads. October 2010.
[31] Pierson, W.J. y Moskowitz, L 1964 “A proposed spectral form for fully developed wind seas based on the similarity theory of S.A. Kitaigorodskii” Journal Geophysical Research, 69, pp. 5181-5190.
[32] Moskowitz, L., W. J. Pierson and E. Mehr, “Wave spectra estimated from wave records obtained by the OWS Weather Explorer and the OWS Weather Reporter”. Parts 1, 2 and 3, Tech. Repts. U. S. Naval Oceanographic OÆce, New York University, 1962.
[33] Komen, G. J., K. Hasselmann, “On the Existence of a Fully Developed Wind-Sea Spectrum”. Journal of physical oceanography, Volume 14, Issue 8, pages: 1271–1285 (August 1984).
[34] Y. Goda. Analysis of Wave Grouping and spectra of Long-travelled Swell, Report of the Port and Harbour. Research Inst., Vol 22, Nº 1. 1983.
[35] Bouws, E., Günther, H., Rosenthal, W. and Vincent, C.L. (1985) Similarity of the wind wave spectrum in finite depth water: 1. Spectral form. J. Geophys. Res., 90, C1, pp. 975-86.
[36] Mitsuyasu, W., 1970, "Development of Spectra of Wind and Waves (2)", Proceedings of the 17th Coastal Engineering Conference, pp.1-7.
[37] J. W. Weber and G.P. Thomas. “An Investigation into the Importance of the Air Chamber Design of an Oscillating Water Column Wave Energy Device”. Proceedings of the 11th International Offshore and Polar Engineering Conference, Stavanger, Norway, 2001.
[38] Falcao, A., Henriques, J.C.C., and Candido, J.J., “Dynamic and optimization of the OWC spar buoy wave energy converter.” Renewable Energy, 2012. 48: p. 369-381.
[39] Sheng, W., Alcorn, R., and Lewis, A., “Assessment of primary wave energy conversions of oscillating water columns.” I. Hydrodynamic analysis. Journal of Renewable and Sustainable Engineering, 2014. 6: p. 053113.
[40] Setoguchi, T., Takao, M.: ‘Current status of self rectifying air turbines for wave energy conversion’, Energy conversion and management, 2006, 47, (15-16), pp. 2382–2396.
[41] Jayashankar, V., Anand, S., Geetha, T., Santhakumar, S., Kumar, V.J., Ravindran, M., et al.: ‘A twin unidirectional impulse turbine topology for owc based wave energy plants’, Renewable energy, 2009, 34, (3), pp. 692–698.